

Effects of rotation and Coulomb type potential on the spin-1/2 Aharonov-Bohm problem

Márcio M. Cunha^{1,*}, Fabiano M. Andrade^{2,3,†} and Edilberto O. Silva^{1,‡}

¹*Departamento de Física, Universidade Federal do Maranhão, 65085-580 São Luís, Maranhão, Brazil*

²*Departamento de Matemática e Estatística, Universidade Estadual de Ponta Grossa, 84030-900 Ponta Grossa, Paraná, Brazil*

³*Programa de Pós-Graduação Ciências/Física, Universidade Estadual de Ponta Grossa, 84030-900 Ponta Grossa, Paraná, Brazil*

(Dated: December 28, 2021)

In this work, we investigate how both rotation and a Coulomb potential affect the quantum mechanical description of a spin-1/2 particle in the presence of the Aharonov-Bohm effect. We employ the method of the self-adjoint extensions in the framework of the Pauli-Schrödinger equation. We discuss the role of the spin degree of freedom on this problem, find the energy spectrum, and investigate the results in detail.

PACS numbers: 03.65.Ge, 03.65.Db, 98.80.Cq, 03.65.Pm

I. INTRODUCTION

The Coulomb interaction has a fundamental relevance in describing several physical systems, covering elementary aspects regarding the electromagnetic theory. Also, it is relevant to study systems that are in the scope of atomic and nuclear physics. In non-relativistic quantum mechanics, the Coulomb potential constitutes a basic example in which we can solve the Schrödinger equation explicitly, in a complete and closed form [1]. More precisely, the Coulomb potential describes the interaction between the electron and the nucleus for hydrogen-like atoms.

Due to its relevance, studying the quantum mechanical description of other systems of interest in the presence of the Coulomb interaction still is an attractive issue nowadays. Besides the usual methods, it is possible, for example, to obtain exact solutions for the one-dimensional Schrödinger equation through the Laplace transform [2]. The nonlinear logarithmic Schrödinger equation in the presence of the Coulomb potential also constitutes an example of a solvable problem in this context [3]. Regarding its application, Coulomb-type potentials can model a wide range of systems in condensed matter physics, like finite crystals [4] and many-body Hamiltonians of nanoscale devices [5], for example. Recent contributions in the literature investigate the role of the Coulomb interaction in the quantum mechanical description of a given system. In particular, we can cite the study of the quantum Drude model [6] and the investigation of decoherence mechanisms which are mediated by the Coulomb interaction [7].

Concerning the fundamental aspects of quantum mechanics, another essential issue that attracts interest in several research lines consists of examining the importance of the Aharonov-Bohm effect (hereafter, AB effect) in the quantum dynamics of a system. The seminal work of Aharonov and Bohm provided a new understanding of the significance of the vector potential in the quantum domain [8]. As a historical and pedagogic remark, it is worth mentioning that Aharonov and Bohm have proposed both a magnetic and an electric ver-

sion of that effect. In the present work, we are interested in the case of the magnetic one. Also, let us have in mind that the AB effect can emerge in two different situations: in the context of interference of the wave function of electrons, for example, when a magnetic flux is present, and also in the case of electrons which are constrained to move in a limited region of space. We can associate the appearance of geometrical phases to the first case, while in the second one, the AB effect alters the bound state energies of the system [9]. These two situations can occur in a wide variety of physical systems. For instance, in condensed matter systems like graphene and carbon nanotubes, the AB effect introduces oscillations in the energy gap of these structures [10, 11]. Also, it is possible to create AB interferometers to perform transport measurements in graphene [12]. The AB effect also can occur in the relativistic domain [13]. It is relevant to mention that the concepts behind the AB effect have inspired the study of analogs such as a gravitational one [14] and a version for neutral particles named the Aharonov-Casher effect [15]. Beyond these topics, we can dedicate attention to aspects concerning fundamental issues involving the AB effect. Currently, there still exists a debate on the origin, interpretations and implications of the AB effect [16–19]. There are also relevant works in the literature on the AB effect applied to other physical systems, for example, problems involving spin and pseudo-spin symmetries [20–28], topological defects [29–35], thermodynamic aspects [36–43], κ -deformed algebra [44, 45], Lorentz symmetry violation [46–49] and Duffin-Kemmer-Petiau (DKP) formalism [50–53]. Another topic of central importance in this context refers to the description of the AB effect by taking into account the electron spin degree of freedom [54]. As we shall see in more detail below, this problem demands particular mathematical tools for adequate treatment [55]. When a magnetic field is present, we know that the spin degree of freedom is responsible for lifting the degeneracy of the energy levels of a particle due to the Zeeman interaction. A similar effect occurs when a system is rotating. More specifically, there is a coupling between the spin degree of freedom and the rotation known as spin-rotation coupling. That coupling also breaks the degeneracy between the different spin eigenvalues. In the context of interferometry, we can consider it as a quantum mechanical extension of the Sagnac effect [56]. In solid state physics, spin-rotation coupling can be a route for

* marciomc05@gmail.com

† fmandrade@uepg.br

‡ edilberto.silva@ufma.br

the generation of spin currents [57]. Another interesting situation occurs in the framework of linearized general relativity, consisting of a spin-rotation-gravity coupling. That quantity allows defining a gravitomagnetic Stern-Gerlach force [58].

In general, studying the effects of rotation on quantum systems is not restricted to spin-rotation coupling, and others aspects are also relevant. Another contribution from rotation appears on the orbital angular momentum, which also appears in the classical scenario. From gravitation and cosmology until the condensed matter physics, rotation effects constitute a fruitful issue for investigation. In this context, rotation can be inherent to the system. It occurs in the case of neutron stars, black holes, and fullerenes, for instance. In a neutral star, rotation powers its electromagnetic activity [59]. Similar behavior occurs in the case of black holes, in which rotation creates processes of ionization and irradiation [60]. Fullerenes spin rapidly at room temperatures, and a laser pulse can transfer angular momentum to C_{60} , affecting lattice properties like phonons [61]. Such molecules also are present in fullerite crystals, having a central role in the crystal behavior [62]. In rotating semiconductors, impressive features emerge. In particular, these systems present a purely quantum mechanical effect, which consists of breaking the equivalence of clockwise/counterclockwise rotations, modifying their mechanical and transport properties [63]. Another example of a system in which this clockwise/counterclockwise asymmetry arises refers to the AB effect for excitons in a semiconductor quantum ring [64].

Considering that both AB effect and rotation can reveal genuinely quantum mechanical effects in a system, it is interesting to investigate the dynamics of a quantum system in the presence of these two features. Besides, due to the role of the spin degree of freedom in producing a Zeeman interaction and the spin-rotation coupling, it is relevant to include it in the problem. Then, in this work, we study the spin-1/2 Aharonov-Bohm problem subjected to rotation and a Coulomb-type interaction. The introduction of the Coulomb potential is also motivated by its vital importance in modeling quantum systems. Since we are interested in examining the nonrelativistic scenario, we work with the Pauli-Schrödinger equation to accommodate the presence of the spin degree of freedom.

The organization of the paper is as follows. In Sec. II, we introduce the Pauli-Schrödinger equation for a rotating frame in the presence of the AB effect and a Coulomb-type potential. By employing the method of the self-adjoint extensions, we solve the corresponding differential equation, obtaining the energy spectrum for the problem. Then, in Sec. III, we focus our attention on analyzing the results, through several graphs of the energy spectrum as a function of the physical parameters of the system. We make our conclusions in Sec. IV.

II. THE PAULI-SCHRÖDINGER EQUATION IN A ROTATING FRAME

The equation that describes the motion of a nonrelativistic spin-1/2 particle in the presence of an electromagnetic field in a rotating frame is the Pauli-Schrödinger equation with the inclusion of the Zeeman energy term, the term describing inertial effects plus the spin-rotation coupling [65]. The corresponding equation is

$$i\hbar \frac{\partial \psi}{\partial t} = \left[\frac{\boldsymbol{\pi}^2}{2m_e} + V(r) - \boldsymbol{\mu} \cdot \mathbf{B} - \boldsymbol{\Omega} \cdot (\mathbf{r} \times \boldsymbol{\pi} + \mathbf{S}) \right] \psi, \quad (1)$$

where $\boldsymbol{\mu} = (e\hbar\mathbf{S}/m_e c)$ is the magnetic moment, m_e is the electron mass, c is the speed of light, e is the electric charge, \hbar is the Planck constant, $\boldsymbol{\Omega}$ is the rotation frequency with respect to an inertial frame, \mathbf{A} is the vector potential, $V(r)$ is the scalar potential and $\boldsymbol{\pi} = \mathbf{p} - e\mathbf{A}/c$ is the mechanical momentum. The spin operator \mathbf{S} is $\hbar\boldsymbol{\sigma}/2$. Also, we assume that the rotation velocity $\boldsymbol{\Omega} \times \mathbf{r}$ is uniform, where \mathbf{r} is the position vector from the origin at the rotation axis. Note that the explicit dependence relative to the spin degree of freedom in Eq. (1) is through the magnetic interaction $\boldsymbol{\mu} \cdot \mathbf{B}$ and the spin-rotation coupling $\boldsymbol{\Omega} \cdot \mathbf{S}$. For the field configuration, we consider the magnetic field of an infinitely long, infinitesimally thin solenoid along the z-axis

$$e\mathbf{B} = e(\nabla \times \mathbf{A}) = \left(0, 0, -\phi \frac{\delta(r)}{r} \right), \quad (2)$$

with r being the two-dimensional radius vector. In the Coulomb gauge, the magnetic field \mathbf{B} is due to the potential vector

$$e\mathbf{A} = \left(0, -\frac{\phi}{r}, 0 \right), \quad (3)$$

where $\phi = \Phi/\Phi_0$ is related to the Aharonov-Bohm flux along the solenoid, in which Φ denotes the magnetic flux and $\Phi_0 = 2\pi/e$ indicates the quantum of magnetic flux. The scalar potential $V(r)$ in Eq. (1) is an attractive Coulomb-type potential given by

$$V(r) = -\frac{\eta}{r}, \quad (4)$$

where η is a real positive parameter describing the strength of the potential. When incorporated into the present model, the potential (4) should be interpreted as being cylindrically symmetric, and it also allows us to obtain analytical solutions to the Pauli-Schrödinger equation (1). For the rotation frequency, we specialize to the case $\boldsymbol{\Omega} = (0, 0, \Omega)$, which is related to the rotation velocity as $\boldsymbol{\Omega} \times \mathbf{r} = \Omega r \hat{\boldsymbol{\varphi}}$. Before solving Eq. (1), we can note that the wave function ψ is an eigenfunction of σ^z , whose eigenvalues are known to be $s = \pm 1$, satisfying $\sigma^z \psi = s\psi = \pm\psi$. For a stationary solution of energy \mathcal{E} of the form

$$\psi(r, \varphi) = e^{-\frac{i\mathcal{E}}{\hbar} t} e^{im\varphi} \mathcal{F}(r), \quad (5)$$

where $m = 0, \pm 1, \pm 2, \pm 3, \dots$ is the angular momentum quantum number, we obtain the radial equation of motion

$$\mathcal{H}\mathcal{F}_m(r) = \kappa^2 \mathcal{F}_m(r), \quad (6)$$

where

$$\mathcal{H} = \mathcal{H}_0 + s\phi \frac{\delta(r)}{r} \quad (7)$$

and

$$\mathcal{H}_0 = -\frac{1}{r} \frac{d}{dr} \left(r \frac{d}{dr} \right) + \frac{j^2}{r^2} - \frac{2m_e \eta'}{r}, \quad (8)$$

$$\kappa^2 = \frac{2m_e \mathcal{E}}{\hbar^2} + \frac{2m_e \Omega}{\hbar} \left(j + \frac{s}{2} \right), \quad (9)$$

$$j = m + \phi, \quad \eta' = \frac{\eta}{\hbar^2}. \quad (10)$$

The radial equation (6) shows up in several articles in the literature and the operator \mathcal{H} is not essentially self-adjoint for all values of j . Here, we characterize the family of self-adjoint extensions of \mathcal{H}_0 , replacing the δ function by a boundary condition at the origin as established in Ref. [66] (see also Refs. [55]). This boundary condition is a mathematical limit that allows divergent solutions for the Hamiltonian \mathcal{H}_0 at isolated regions, provided they remain square-integrable. For the present model, the access to such isolated regions is conditioned by the relation [67]

$$|j| < \frac{1}{2}, \quad (11)$$

which evidences the region where the operator \mathcal{H}_0 is essentially self-adjoint, i.e., $|j| \geq 1/2$. From Eq. (10), we see that the isolated regions depend on the values of ϕ . Then, by decomposing the magnetic quantum flux as

$$\phi = N + \beta, \quad (12)$$

with N being the largest integer contained in ϕ , and the quantity β being defined in the range

$$0 \leq \beta < 1, \quad (13)$$

we find an expression for the angular momentum quantum number m satisfying the relation (11), which is given by

$$-\frac{1}{2} - (N + \beta) < m < \frac{1}{2} - (N + \beta), \quad (14)$$

and it shows the range of m in which \mathcal{H}_0 is not self-adjoint. In view of the above information, it is evident that the radial equation (6) must be solved taking into account the relation (11). In this way, all the self-adjoint extensions $\mathcal{H}_{0, \lambda_m}$ of \mathcal{H}_0 are characterized by the boundary condition at the origin [66]

$$\lambda_m \mathcal{F}_0 = \mathcal{F}_1, \quad (15)$$

with $-\infty < \lambda_m \leq \infty$, $-1/2 < j < 1/2$ and the boundary values are given by

$$\begin{aligned} \mathcal{F}_0 &= \lim_{r \rightarrow 0^+} r^{|j|} \mathcal{F}_m(r), \\ \mathcal{F}_1 &= \lim_{r \rightarrow 0^+} \frac{1}{r^{|j|}} \left[\mathcal{F}_m(r) - \mathcal{F}_0 \frac{1}{r^{|j|}} \right]. \end{aligned} \quad (16)$$

It is important to emphasize that when $\lambda_m = \infty$, it means that we are dealing with the free Hamiltonian without the point interaction. In this case, the wave function is regular at the origin, and the original AB problem [68] is recovered. For any other values of λ_m , i.e., $|\lambda_m| < \infty$, the Hamiltonian characterizes a singularity at $r = 0$ region. As a result, the boundary condition admits a $r^{-|j|}$ singularity in the wave functions at this point [69]. This is a well-known result in the literature.

It can be shown that Eq. (5) is of the confluent hypergeometric equation type, whose general solution is given in terms of the Kummer function $M(a, b, z)$ and the confluent hypergeometric function of the second kind $U(a, b, z)$. A convenient expression for dealing with this solution is achieved by making use of properties allowing us to write the confluent hypergeometric function of the second kind in terms of Kummer functions (or confluent hypergeometric function of the first kind ${}_1F_1(a, b, z)$). In this way, we express the solution of Eq. (5) in the form

$$\begin{aligned} \mathcal{F}_m(x) &= a_m x^{|j|} e^{-\frac{x}{2}} {}_1F_1(a, b, x) \\ &\quad + b_m x^{-|j|} e^{-\frac{x}{2}} {}_1F_1(a', b', x), \end{aligned} \quad (17)$$

with

$$x = 2\kappa r, \quad (18)$$

$$a = \frac{1}{2} + |j| - \frac{m_e \eta'}{\kappa}, \quad b = 1 + 2|j|, \quad (19)$$

$$a' = \frac{1}{2} - |j| - \frac{m_e \eta'}{\kappa}, \quad b' = 1 - 2|j|, \quad (20)$$

where a_m and b_m are, respectively, the coefficients of the regular and irregular solutions at the origin. Note that in the case of bound state solutions, it must be ensured that the function $e^{-x/2}$ is convergent when $x = \infty$. Thus, we write the quantity κ^2 in Eq. (9) as

$$\kappa = \sqrt{-\left[\frac{2m_e \mathcal{E}}{\hbar^2} + \frac{2m_e \Omega}{\hbar} \left(j + \frac{s}{2} \right) \right]}, \quad (21)$$

with the requirement that

$$\frac{2m_e \mathcal{E}}{\hbar^2} + \frac{2m_e \Omega}{\hbar} \left(j + \frac{s}{2} \right) < 0 \quad (22)$$

to guarantee that κ is a real quantity. With the condition (22), the exponential function $e^{-x/2}$ tends to zero when $x \rightarrow \infty$. On the other hand, if

$$\frac{2m_e \mathcal{E}}{\hbar^2} + \frac{2m_e \Omega}{\hbar} \left(j + \frac{s}{2} \right) > 0, \quad (23)$$

the exponential $e^{-x/2}$ oscillates when $x \rightarrow \infty$.

Our main goal is to obtain an expression for bound state energies. We make that through two stages. In the first one, we must substitute the solution (17) into the boundary condition (15), which should provide a relation between the coefficients a_m and b_m . In the second stage, we require that the solution be normalizable at large r . From this condition, we can obtain another relation between the coefficients a_m and b_m . Combining the two relations involving such coefficients makes it

possible to find a secular equation that provides the energies of the bound states. The two procedures are performed as follows. Since the boundary condition is applied at the $r = 0$ region, we must use series expansions up to second order in the argument to the functions $e^{-x/2}$ and ${}_1F_1(a, b, x)$. After combining the results, we get

$$e^{-\frac{x}{2}} {}_1F_1(a, b, x) \approx \frac{(x^2 - 4x + 8)}{16b(b+1)} \times [(a^2 + a)x^2 + 2(ax + b)(b+1)]. \quad (24)$$

With this result, the solution (17) takes the form

$$\begin{aligned} \mathcal{F}_m(x) = & a_m \frac{(x^2 - 4x + 8) x^{|j|}}{16b(b+1)} \\ & \times [(a^2 + a)x^2 + 2(ax + b)(b+1)] \\ & + b_m \frac{(x^2 - 4x + 8) x^{-|j|}}{16b(b+1)} \\ & \times [(a'^2 + a')x^2 + 2(a'x + b')(b'+1)]. \quad (25) \end{aligned}$$

Substituting the solution (25) into the boundary condition (15) and separating the terms involving the limits that require some criterion for their realization, we find

$$\begin{aligned} b_m (2\kappa)^{-|j|} = & \lambda_m \\ & \times \left[a_m (2\kappa)^{|j|} + b_m (2\kappa)^{1-|j|} \left(\frac{a'}{b'} - \frac{1}{2} \right) \lim_{r \rightarrow 0^+} r^{1-2|j|} \right] \\ & + \lambda_m \left[b_m \frac{1}{2} (2\kappa)^{2-|j|} \left(\frac{1}{4} - \frac{a'}{b'} + \frac{a'}{b'^2 + b'} + \frac{a'^2}{b'^2 + b'} \right) \right. \\ & \left. \times \lim_{r \rightarrow 0^+} r^{2-2|j|} \right]. \quad (26) \end{aligned}$$

It is possible to recover results from the literature through Eq. (26). For this purpose, it is more convenient to write it in the form

$$\begin{aligned} b_m (2\kappa)^{-2|m+\phi|} = & a_m \lambda_m \\ & - \lambda_m b_m (2\kappa)^{-2|m+\phi|} \left(\frac{2\eta' m_e}{2|m+\phi| - 1} \right) \lim_{r \rightarrow 0^+} r^{1-2|m+\phi|} \\ & + b_m \frac{\lambda_m}{4} \left(\frac{\kappa^2 - 2\kappa^2|m+\phi| + 4\eta'^2 m_e^2}{2|m+\phi|^2 - 3|m+\phi| + 1} \right) (2\kappa)^{-2|m+\phi|} \\ & \times \lim_{r \rightarrow 0^+} r^{2-2|m+\phi|}. \quad (27) \end{aligned}$$

In the absence of a Coulomb potential, it is known that the wave functions are given in terms of Bessel functions. Since it is possible to express the Bessel functions in terms of the confluent hypergeometric function, we can recover the expected result by setting $\eta' = 0$ in Eq. (27). We obtain

$$\begin{aligned} a_m \lambda_m = & b_m (2\kappa)^{-2|m+\phi|} \\ & \times \left[1 - \lambda_m \frac{\kappa^2}{4(1 - |m+\phi|)} \lim_{r \rightarrow 0^+} r^{2-2|m+\phi|} \right]. \quad (28) \end{aligned}$$

The occurrence of a regular solution directly implies that $b_m = 0$ (or $\lambda_m = 0$) in Eq. (28). In contrast to this case, the occurrence of a singular solution demands that $|m + \phi| < 1$, and the relation between the coefficients yields $a_m/b_m \sim \lim_{r \rightarrow 0^+} r^{2-2|m+\phi|}$. As expected, this result coincides with Eq. (15) of Ref. [70] by making $r = R$. Furthermore, it is also important to mention that Eq. (28) reveals us that the range of $|m + \phi|$ is increased in the absence of the Coulomb potential. Equation (28) also can be compared with Eq. (64) of Ref. [71]. For this to be accomplished, we must restore the parameters $\kappa \rightarrow ik$ and $m + \phi \rightarrow [m + \phi + (1 - \alpha)/2]/\alpha$ and then multiplying the resulting equation by $(2\kappa)^{-|m+\phi|}$. This leads to the expression

$$\begin{aligned} a_m \lambda_m = & b_m (2ik)^{-\frac{2}{\alpha}[m+\phi+\frac{1}{2}(1-\alpha)]} \\ & \times \left[1 + \frac{\lambda_m k^2}{4(1 - \frac{1}{\alpha}[m+\phi+\frac{1}{2}(1-\alpha)])} \right] \\ & \times \lim_{r \rightarrow 0^+} r^{2-\frac{2}{\alpha}[m+\phi+\frac{1}{2}(1-\alpha)]}, \quad (29) \end{aligned}$$

which is just Eq. (64) of Ref. [71].

Returning to our problem and analyzing the limits in Eq. (27), we find that the relevant one has the lowest power in r , which allows us to neglect $\lim_{r \rightarrow 0^+} r^{2-2|j|}$. After simplifying the resulting expression, we obtain

$$a_m \lambda_m (2\kappa)^{2|j|} = b_m \left[1 + \left(\frac{2\lambda_m m_e \eta'}{1 - 2|j|} \right) \lim_{r \rightarrow 0^+} r^{1-2|j|} \right]. \quad (30)$$

Notice that $\lim_{r \rightarrow 0^+} r^{1-2|j|}$ is convergent if $|j| < 1/2$ and diverges if $|j| \geq 1/2$, thus revealing the condition for the occurrence of a singular solution at the origin. In other words, this means that for $|j| \geq 1/2$ the coefficient b_m is zero, which implies that only the regular solution at the origin should be considered in the solution [71–77]. It is also known that the occurrence of singular solutions is a consequence of the fact that the operator \mathcal{H}_0 is not self-adjoint for the condition $|j| < 1/2$.

Let us now perform the second stage in order to find the second relation between a_m and b_m . Since the requirement to ensure that the wave function is normalizable is $\lim_{x \rightarrow \infty} \mathcal{F}_m(x) = 0$, we use the asymptotic representation of the function ${}_1F_1(a, b, x)$ for large x

$${}_1F_1(a, b, x) = \frac{\Gamma(b)}{\Gamma(a)} e^x x^{a-b} + \frac{\Gamma(b)}{\Gamma(b-a)} (-x)^{-a}, \quad (31)$$

which substituted into solution (17), results

$$\begin{aligned} \lim_{x \rightarrow \infty} \mathcal{F}_m(x) = & \\ & a_m x^{|j|} e^{-\frac{x}{2}} \left[\frac{\Gamma(b)}{\Gamma(a)} e^x x^{a-b} + \frac{\Gamma(b)}{\Gamma(b-a)} (-x)^{-a} \right] \\ & + b_m x^{-|j|} e^{-\frac{x}{2}} \left[\frac{\Gamma(b')}{\Gamma(a')} e^x x^{a'-b'} + \frac{\Gamma(b')}{\Gamma(b'-a')} (-x)^{-a'} \right] \\ & = 0. \end{aligned}$$

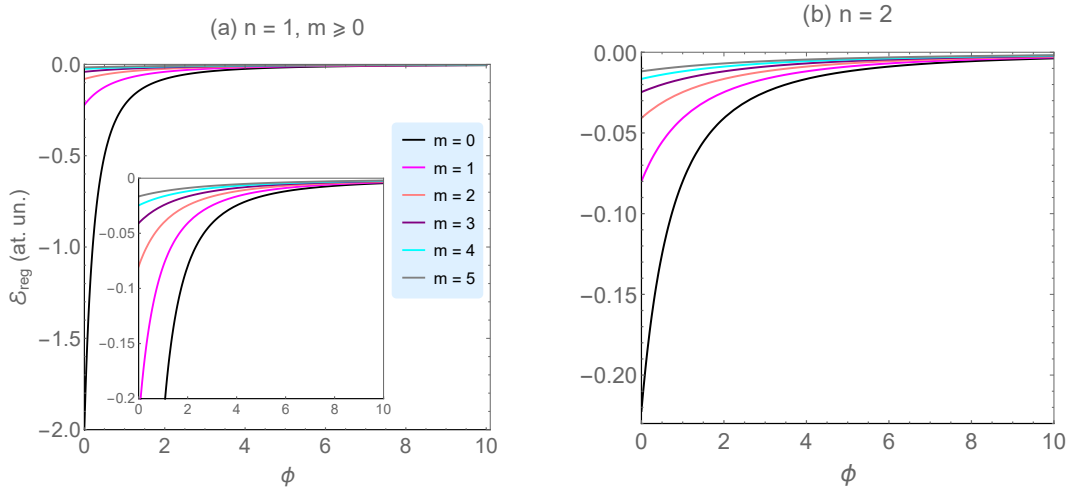


FIG. 1. (Color online) Energy of the regular case (Eq.(35)) as a function of ϕ without taking into account rotation effects ($\Omega = 0$) for $m \geq 0$. In panel (a), we plot for $n = 1$ and in panel (b) for $n = 2$. The energy of the ground state for a specific value of m tends to zero as the flux increases. For $n = 2$, we see clearly that the effects manifested in (a) tend to occur more rapidly.

Neglecting the terms involving functions that diverge on the $x \rightarrow \infty$ limit and simplifying the result, we arrive at the following relation:

$$a_m \Gamma(b) \Gamma(b' - a') + b_m \Gamma(b') \Gamma(b - a) = 0, \quad (32)$$

which can be written more explicitly as

$$a_m \Gamma(1 + 2|j|) \Gamma\left(\frac{1}{2} - l_-\right) + b_m \Gamma(1 - 2|j|) \Gamma\left(\frac{1}{2} + l_+\right) = 0, \quad (33)$$

where we have defined the parameters $l_+ = |j| + m_e \eta' / \kappa$ and $l_- = |j| - m_e \eta' / \kappa$. Equation (33) is the second relation between a_m and b_m that we need.

Finally, combining the relations (30) and (33), we obtain

$$\lambda_m (2\kappa)^{|j|} \frac{\Gamma(1 - 2|j|)}{\Gamma(\frac{1}{2} - l_-)} + (2\kappa)^{-|j|} \frac{\Gamma(1 + 2|j|)}{\Gamma(\frac{1}{2} + l_+)} = 0. \quad (34)$$

For a given value of the self-adjoint extension parameter λ_m it is possible to determine an expression for the energy of the particle from the poles of the functions $\Gamma(1/2 - l_-)$ and $\Gamma(1/2 + l_+)$ [78, 79]. The values of λ_m we have chosen are $\lambda_m = 0$ and $\lambda_m = \infty$, which are justified by the requirement that the wave function must be well behaved at these limit values. For the choice $\lambda_m = 0$, it means that the Hamiltonian is free of singularities. In this case, the regular solution is the bound state wave function. On the other hand, if $\lambda_m = \infty$, only the irregular solution contributes to the bound state wave function.

III. DISCUSSION OF THE RESULTS

For all other values of λ_m , both regular and irregular solutions contribute to the bound state wave function. The expres-

sions for the energies corresponding to each case are given by

$$\mathcal{E}_{\text{reg}} = -\frac{1}{2\hbar^2} \frac{m_e \eta^2}{\left(n - \frac{1}{2} + |m + N + \beta|\right)^2} - \hbar \Omega \left(m + N + \beta + \frac{s}{2}\right), \quad (\text{for } \lambda_m = 0), \quad (35)$$

$$\mathcal{E}_{\text{irreg}} = -\frac{1}{2\hbar^2} \frac{m_e \eta^2}{\left(n - \frac{1}{2} - |m + N + \beta|\right)^2} - \hbar \Omega \left(m + N + \beta + \frac{s}{2}\right), \quad (\text{for } \lambda_m = \infty), \quad (36)$$

with $n = 1, 2, \dots$, $N = 0, 1, 2, \dots$ and $0 \leq \beta < 1$. Notice that the rotation implies a shift in the energy levels. Depending on the values of m and s , this shift can be either up or down. For $\Omega = 0$, $\hbar = 1$, and then readjusting the notation for the parameters, we recover the expressions for the energies obtained in Refs. [67, 70, 80]. In the absence of the spin degree of freedom, we recover the result for the case of regular solution at the origin [81].

In this section, we study in detail the effects of the spin degree of freedom, the AB flux, and the intensity of the Coulomb potential on the energy levels of the particle. Analyzing the expressions for the energies (35) and (36), we see that they depend explicitly on the quantities n , m , ϕ , η , Ω and s .

We shall show in detail, through graphical illustrations, that the system can assume different configurations of states of energies for a specific set of these parameters. An immediate realization that can be verified in (35) and (36) is that in the absence of rotation, the resulting equations are just the results known in the literature, from which is found that all energy eigenvalues are negative. Under rotation effects, we see that the energies contain an additional linear term that explicitly depends on Ω . With the presence of this term, all energy levels are shifted, either up or down, depending on the parameter values. An interesting feature in this model that we will show

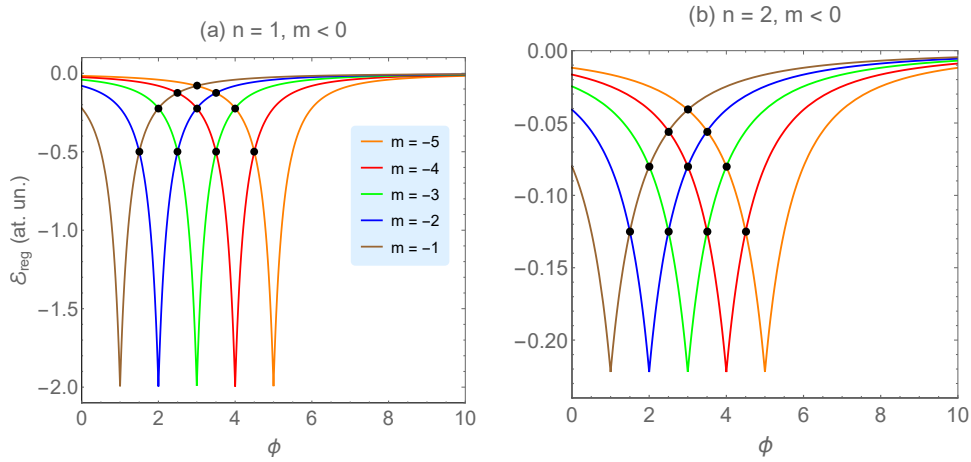


FIG. 2. (Color online) Energy of the regular case (Eq. (35)) as a function of the Aharonov-Bohm flux without taking into account rotation effects ($\Omega = 0$) for $m < 0$. In panel (a), we plot for $n = 1$ and in panel (b) for $n = 2$. In (a), \mathcal{E}_{reg} increases with the flux and has maximum magnitude for integer values of ϕ . The maximum value of \mathcal{E}_{reg} is the same for all states with $m < 0$. In the first excited state, we verify that only the location of the degenerate states is changed on the energy scale (panel (b)).

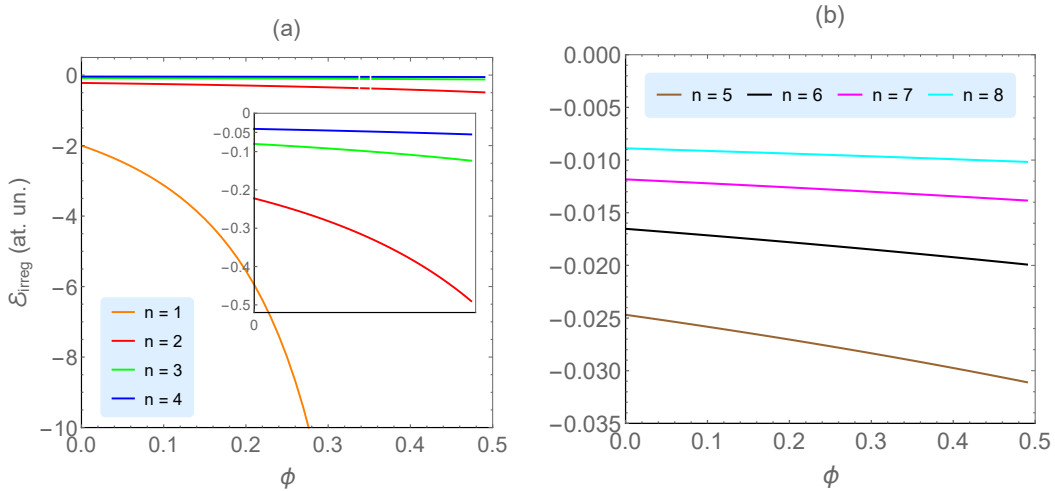


FIG. 3. (Color online) Plots of $\mathcal{E}_{\text{irreg}}$ (Eq. (36)) as a function of ϕ without taking into account rotation effects ($\Omega = 0$). In (a) the first four energy levels of (1) as a function of ϕ for $m = 0$. The magnitude of the energy of the ground state is much larger than that of the other levels ($n = 2$ (solid red line), $n = 3$ (solid green line) and $n = 4$ (solid blue line)) for any value of ϕ in the range considered. At $\phi = 0.49$, $\mathcal{E}_{\text{irreg}, n=1}$ (solid orange line) exhibits a magnitude of -5×10^3 . In (b), the energy levels with $n = 5$ (solid brown line), $n = 6$ (solid black line), $n = 7$ (solid magenta line) and $n = 8$ (solid cyan line). The spacing between the energy levels with $n > 5$ decreases with increasing n , and $|\mathcal{E}_{\text{irreg}}|$ increases with ϕ .

later is that this shift leads to some positive energy values. Without a more detailed analysis, this feature is not so evident when we look at the expressions for the energies. In all our figures and discussions below, we use atomic units $\hbar = 1$, $\eta = 1$ and $m_e = 1$.

We first investigate the energy as a function of the AB flux ϕ for some values of m and n (see Fig. 1) for $\Omega = 0$. For $n = 1$ and $m \geq 0$, we see that $|\mathcal{E}_{\text{reg}}|$ increases for smaller

values of m , which allows us to confirm that the state of the system of highest energy is the one with $m = 0$. For $n = 2$, the curves maintain the same behavior, implying only a decreasing in $|\mathcal{E}_{\text{reg}}|$. For values of ϕ close to 10, the energies tend to zero. For $n = 1$ and $m \leq 0$, we observe a periodic pattern in the energies, which occurs whenever the flux takes on an integer value and the minimum allowed energy is $\mathcal{E}_{\text{reg}} = -2.0$ [see Fig. 2(a)]. We also see the presence

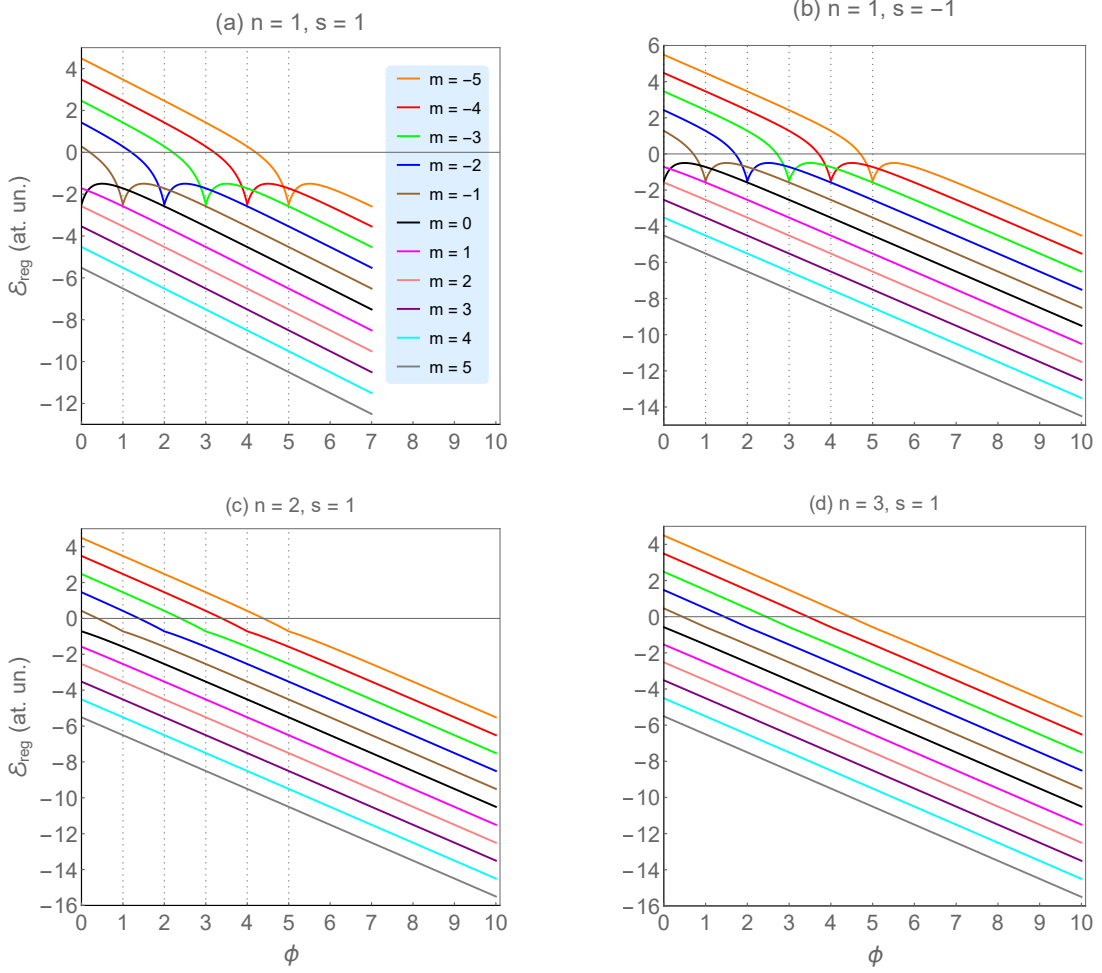


FIG. 4. (Color online) Plots of \mathcal{E}_{reg} (Eq. (35)) as a function of ϕ considering effects of rotation for some values of m . The rotation has the effect of shifting the energy spectrum, allowing positive energies values. The energy states with $n = 1$ and $m \leq 0$ exhibit a partially linear profile due to the combined effects between the magnitudes of the Coulomb-type potential and rotation. In (a), the profile for $s = +1$ and (b) for $s = -1$. In the first excited state ($n = 2$), the effects due to the Coulomb-type potential are weak (panel (c)). For $n \geq 3$, the rotation effects are predominant in all range of ϕ , and the profile is completely linear (panel (d)). Independent of the values of the parameters, we see that all energy levels with $m > 0$ are negative and \mathcal{E}_{reg} increases with ϕ while for states with $m < 0$, \mathcal{E}_{reg} decreases with ϕ .

of degenerate states for different values of m , and their number increases when we consider more states and the degenerated energies are schematically indicated by black circles. For $n = 2$ and $m \leq 0$, the pattern of the energy curves is similar but presents a reduction in the scale. It implies a change in the location of the degeneracy points [see Fig. 2(b)]. We observe no change in the number of degenerate states in this case. The position of the degenerate states suffers a shift because of the change in energy scale, from the state $n = 1$ to the state $n = 2$.

To analyze the plot of $\mathcal{E}_{\text{irreg}}$ as a function of ϕ for $\Omega = 0$, we must take into account the allowed range for $|j| = |m + \phi|$ in Eq. (11). It leads to a reduction in the range of ϕ to values smaller than 0.5 (see Fig. 3). Consequently, the only value allowed for m is 0. In Fig. 3(a), we plot the first four energy levels of $\mathcal{E}_{\text{irreg}}$ as a function of ϕ . Notably, one can see that only the ground state (solid orange line) has a magnitude that increases rapidly with ϕ , following this pattern up to the value

$\phi = 0.49$. For energy levels with $n = 2$ (red solid line), $n = 3$ (green solid line) and $n = 4$ (blue solid line), we see that they have the same order of magnitude. The inset in the figure further illustrates this feature. For energy levels with $n \geq 5$, we observe a tendency for them to approach each other, with $|\mathcal{E}_{\text{irreg}}|$ increasing with ϕ [see Fig. 3(b)].

When including rotation effects, i.e., for $\Omega > 0$, depending on the values of the parameters involved, both \mathcal{E}_{reg} and $\mathcal{E}_{\text{irreg}}$ can assume positive or negative values. In Fig. 4, we plot the ground state ($n = 1$) for $s = \pm 1$ [see Figs. 4(a) and 4(b), respectively], and the first ($n = 2$) and second ($n = 3$) excited states for $s = +1$ [see Figs. 4(c) and 4(d), respectively] in the range $m = [-5, +5]$. Since the term involving the rotation in the energies (35) and (36) is linear, its effect corresponds to a shift in the energy scale, depending on the values of the parameters involved. All energies with $m < 0$ start from positive values and decrease as the flux is increased. This behavior continues until the flux reaches an integer value (represented

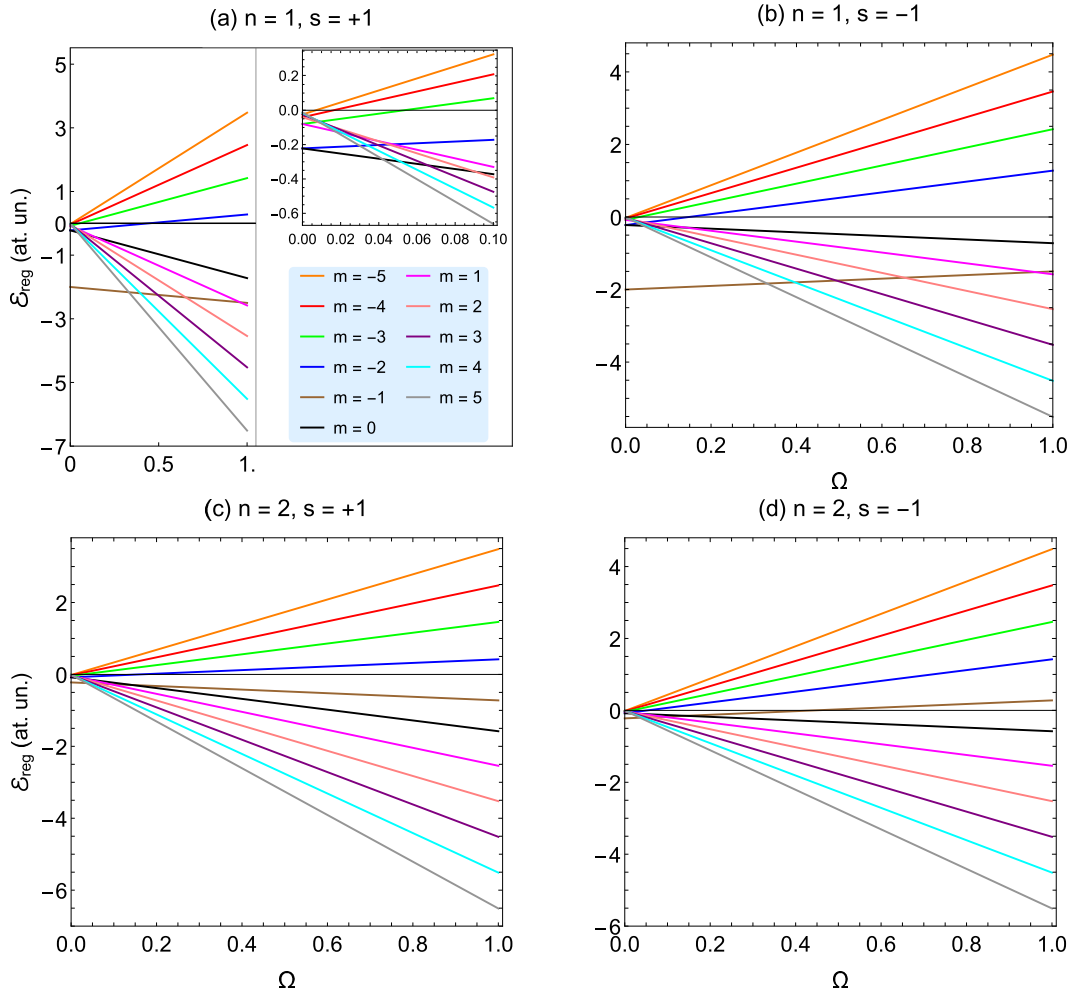


FIG. 5. (Color online) Plots of \mathcal{E}_{reg} (Eq. (35)) as a function of Ω for $n = 1$, $n = 2$, $s = \pm 1$ and some values of m . In all profiles, we have a linear behavior along the range of Ω . All energies with $m = [-5, +5]$ have negative values for flux near zero (see the inset in Fig. (a)). The energy of the ground state with $m = -1$ (Brown solid line) and $s = +1$ has all negative values while for $s = -1$ these energy levels can take on both positive (the region with these values is not displayed on the plot) and negative values (panel (b)). For the first excited state (Figs. (c) and (d)), this characteristic is still present in the spectrum, and $|\mathcal{E}_{\text{reg}}|$ increases with Ω , but $|\mathcal{E}_{\text{reg}} > 0| < |\mathcal{E}_{\text{reg}} < 0|$. In (d), we see more clearly that the energy with $m = -1$ takes on both positive and negative values.

by vertical dashed lines in Fig 4). Continuing by increasing the flux, we observe a slight tendency of decreasing in the $|\mathcal{E}_{\text{reg}}|$, until it returns again to its previous behavior. Note that this effect occurs for all energy levels with $m < 0$. This occurs most explicitly in Figs. 4(a) and 4(b). It can be clarified by analyzing the behavior of $(n - \frac{1}{2} + |m + N + \beta|)^{-2}$ together with the flux decomposition $\phi = N + \beta$ defined in Eq. (12). In fact, this profile was displayed in Fig. 2 where we analyzed the case $\Omega = 0$. For states with $m > 0$, $|\mathcal{E}_{\text{reg}}|$ increases linearly as a function of ϕ . It is also important to note that when $s = -1$ the energy levels are only shifted [see Fig. 4(b)]. When we access the energies of states with $n = 2$, the profile of \mathcal{E}_{reg} tends to be partially linear (observe the regions where the flux assumes integer values in Fig. 4(c)), while for states with $n \geq 3$ it is predominantly linear [see Fig. 4(d)].

As argued above, the term that explicitly depends on rotation in the energies (35) and (36) is linear. Therefore, this

term should be dominant in the spectrum for certain set of parameters. In Figs. 5(a)-(b) we plot the ground state and the first excited state in Figs. 5(c)-(d) of \mathcal{E}_{reg} as a function of Ω for $s = \pm 1$ and some values of m . As we can see, $|\mathcal{E}_{\text{reg}}|$ increases with Ω at almost all energy levels. Moreover, they all start from negative values [see the inset in Fig. 5(a)], but some states follow a tendency to assume positive values (case of the states with $m \leq -2$) and others to negative values (case of the states with $m \geq -1$). In particular, we find that in the first excited state for $s = +1$ [solid brown line in Fig.5(c)] the effects of rotation on the state with $m = -1$ follows the tendency to assume increasingly negative values while for $s = -1$ [solid brown line in Fig. 5(d)] it starts with negative values, and at the end of the range of Ω it takes on positive values.

We also plot in (Fig. 6) the behavior of \mathcal{E}_{reg} as a function of m for $\Omega = 1$, $s = \pm 1$ and some values of ϕ . In Fig. 6(a), we use $\phi = 1$ (blue color), $\phi = 5$ (red color) and $\phi = 10$ while

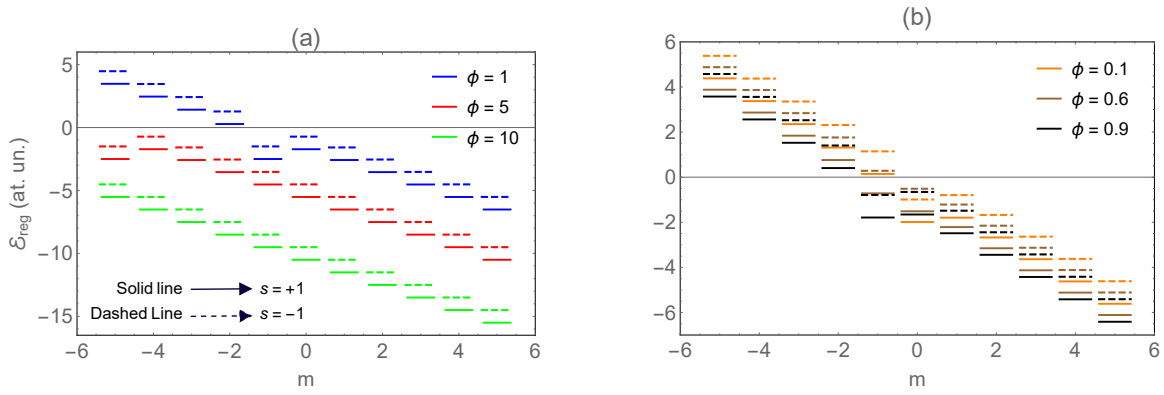


FIG. 6. (Color online) Discrete plots of \mathcal{E}_{reg} (Eq. (35)) as a function of m for some values of ϕ . In Fig. (a), we use $\phi = 1$ (blue color), $\phi = 5$ (red color) and $\phi = 10$ while in Fig. (b), we assume $\phi = 0.1$ (orange color), $\phi = 0.6$ (brown line) and $\phi = 0.9$ (black color). In both profiles, the solid lines denote the states with $s = +1$ and the dashed lines the states with $s = -1$. Degenerate states are present when we compare the profiles for the energies different values of element of spin along the horizontal axis (m axis).

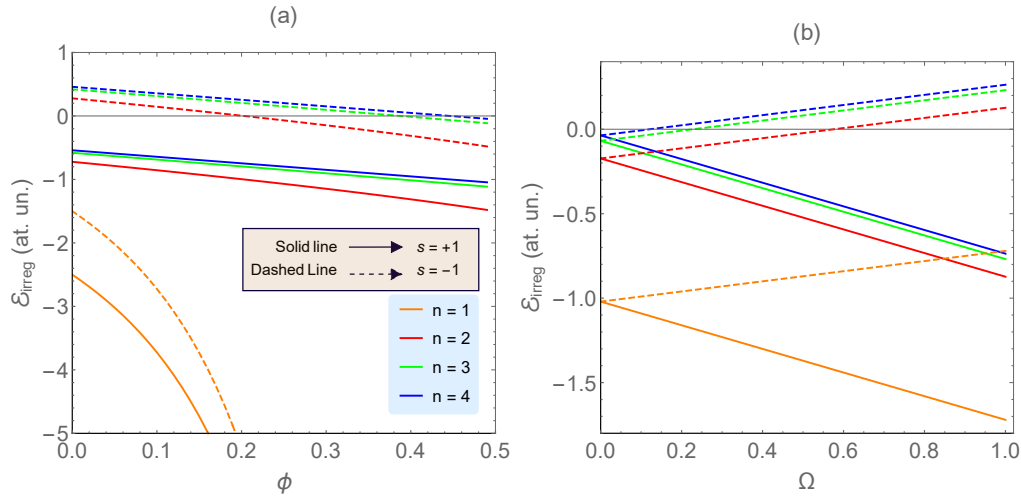


FIG. 7. (Color online) Plots of $\mathcal{E}_{\text{irreg}}$ (Eq.(36)) as a function of ϕ for $m = 0$ (Fig. (a)) and as a function of Ω (Fig. (b)) for $s = \pm 1$ and some values of n . In (a), the ground state for $s = \pm 1$ (solid and dashed orange lines) increases to the value $\phi = 0.49$. The energies (for $s = +1$) with $n = 2$ (solid red line), $n = 3$ (solid green line) and $n = 4$ (solid blue line) are negative and have predominantly linear behavior with ϕ . In Fig. (b), the profile of $\mathcal{E}_{\text{irreg}}$ is linear with Ω . For $s = +1$, all energies are negative. For $s = -1$, only the energy with $n = 1$ is fully negative, while the other energy levels contain both positive and negative values.

in Fig. 6(b), we assume $\phi = 0.1$ (orange color), $\phi = 0.6$ (brown color) and $\phi = 0.9$ (black color). In this figures, the solid lines denote the states with $s = +1$ and the dashed lines the states with $s = -1$. By comparing the profiles of the solid and dashed lines (on the horizontal axis) at the different flux values, we can see the presence of degenerate states when $s = \pm 1$.

Since the effective angular momentum in the energies of the irregular solution satisfies relation (14), then the most interesting plots we can realize are the ones as a function of the AB flux and the rotation. In Fig. 7(a), we plot $\mathcal{E}_{\text{irreg}}$ as a function of ϕ (in the range $|\phi| \leq 0.49$) for $m = 0$ and $s = \pm 1$. We can see that the ground state (solid and dashed orange lines) increases with ϕ up to the value 0.49, point in which it exhibits a magnitude of the order of -5×10^3 . For energy levels with $n \geq 2$ (solid red, green and blue lines) and $s = +1$,

the energies are negative and $|\mathcal{E}_{\text{irreg}}|$ increases with ϕ . In contrast, when $s = -1$, we find positive energies (dominance of rotation effects), with $|\mathcal{E}_{\text{irreg}}|$ decreasing until it reaches zero magnitude (dashed red, green and blue lines). Continuing by increasing the flux, we find that $|\mathcal{E}_{\text{irreg}}|$ increases until the end of the range of ϕ . Finally, when we plot the profile of $\mathcal{E}_{\text{irreg}}$ as a function of Ω , we see a linear behavior (Fig.7(b)). To make this plot agree with relation (14), we use $m = 0$ and $\phi = 0.2$. Note that $|\mathcal{E}_{\text{irreg}}|$ for $n = 1$ and $s = +1$ increases when Ω is increased, with $|\mathcal{E}_{\text{irreg}}|$ being the most energetic state. On the other hand, the profile of $\mathcal{E}_{\text{irreg}}$ for $s = -1$ has energy levels which include both positive and negative values for $n = 2$ (dashed red line), $n = 3$ (dashed green line) and $n = 4$ (dashed blue line) in Fig.7(b). In this configuration, only the ground state (dashed orange line) has negative energy values, and therefore $\mathcal{E}_{\text{irreg}}$ decreases with ϕ .

From the above discussions and graphical illustrations, it is evident that both the spin degree of freedom and rotation has crucial physical implications on its energy spectrum. The combined effects between centrifugal forces and spin element projection lead to various changes in energy levels, such as the appearance of positive energy eigenvalues and localized peaks of low and high magnitudes of energies.

IV. CONCLUSIONS

In this paper, we have studied the spin-1/2 Aharonov-Bohm problem in the presence of a Coulomb type potential in a rotating frame. One of the main goals of this study was to investigate the role of the spin degree of freedom, Coulomb-type interaction, and rotation on the energy levels of the particle. For this to be accomplished, we have considered the Pauli-Schrödinger equation of motion to the order of $1/m_e$, which contains the spin-independent energy (kinetic energy and potential energy) and the interaction energy (magnetic dipole energy, spin-rotation coupling, and the energy due to inertial effects). We have argued that the radial equation of motion contains a singularity in the $r = 0$ region. A technique based on the self-joint extension method was used to deal with this issue. Then, we have solved the problem for bound states and obtained expressions for energy levels of the particle (Eqs. (35) and (36)). These expressions represent the energy levels obtained from the regular and irregular solutions at the origin, respectively. We have investigated these energy levels as a function of the parameters involved from several aspects. We first analyzed the case without rotation effects, focusing only on the effects due to the Zeeman-type term, which leads to the point interaction at the origin. For the energy of the regular solution, we found that $|\mathcal{E}_{\text{reg}}|$ for $n = 1$ and $m \geq 0$ decreases as the flux is increased. This effect occurs most quickly when the particle is in the first excited state. For states with $n = 1$ and $m < 0$, we have verified that $\mathcal{E}_{\text{reg}} \leq -2.0$ with the occurrence of degenerate states while for states with $n = 2$ and $m < 0$, we found that $\mathcal{E}_{\text{reg}} \leq -0.25$

and with the same number of degenerate states. For the energy of the irregular solution $\mathcal{E}_{\text{irreg}}$, we have shown that the states exhibiting the largest magnitudes are the states with $n \leq 4$. When we take into account the effects of rotation, \mathcal{E}_{reg} as a function of ϕ exhibits both positive and negative eigenvalues for $m \leq -1$ and only negative eigenvalues for $m \geq 0$. We also argued that only the ground state contains degenerate states. We have also analyzed the profile of \mathcal{E}_{reg} as a function of the rotation parameter Ω for $n = 1$, $s = \pm 1$ and some values of m . We have found that for $m \leq -2$ both positive and negative eigenvalues are allowed while for $m \geq -1$ only negative eigenvalues appear. These features are also present in the energies of the first excited state for $s = 1$ and $s = -1$. We also found the presence of degenerate states in the profile of \mathcal{E}_{reg} as a function of m for some values of ϕ . We finalized the work by investigating the profiles of $\mathcal{E}_{\text{irreg}}$ as a function of ϕ and Ω for $s = \pm 1$ and some values of n . In the first case, we found that only the energy of the ground state does not exhibit a linear behavior with ϕ . In the second profile, as already expected, the behavior is linear with Ω , and some levels contain both positive and negative energy values.

ACKNOWLEDGMENTS

This work was partially supported by the Brazilian agencies CAPES, CNPq and FAPEMA. FMA also acknowledges CNPq Grants No. 434134/2018-0, and No. 314594/2020-5. EOS acknowledges CNPq Grant No. 307203/2019-0, and FAPEMA Grant No. 01852/14. This study was financed in part by the Coordenação de Aperfeiçoamento de Pessoal de Nível Superior - Brasil (CAPES) - Finance Code 001.

REFERENCES

-
- [1] H. J. W. Müller-Kirsten, *Introduction to Quantum Mechanics*, 2nd ed. (WORLD SCIENTIFIC, 2012) <https://www.worldscientific.com/doi/pdf/10.1142/8428>.
 - [2] Y. Ran, L. Xue, S. Hu, and R.-K. Su, *J. Phys. A* **33**, 9265 (2000).
 - [3] T. C. Scott and J. Shertzer, *J. Phys. Commun.* **2**, 075014 (2018).
 - [4] L. N. Kantorovich and I. I. Tupitsyn, *J. Phys.: Condens. Matter* **11**, 6159 (1999).
 - [5] G. Albareda, J. Suñé, and X. Oriols, *Phys. Rev. B* **79**, 075315 (2009).
 - [6] M. Sadhukhan and F. R. Manby, *Phys. Rev. B* **94**, 115106 (2016).
 - [7] N. Kerker, R. Röpke, L. M. Steinert, A. Pooch, and A. Stibor, *New J. Phys.* **22**, 063039 (2020).
 - [8] Y. Aharonov and D. Bohm, *Phys. Rev.* **115**, 485 (1959).
 - [9] M. Peshkin, *Phys. Rev. A* **23**, 360 (1981).
 - [10] J. Schelter, D. Bohr, and B. Trauzettel, *Phys. Rev. B* **81**, 195441 (2010).
 - [11] H. Chen, E. Zhang, K. Zhang, and S. Zhang, *RSC Adv.* **5**, 45551 (2015).
 - [12] X. Wei, W.-J. Zhang, and S.-G. Cheng, *J. Phys.: Condens. Matter* **30**, 485302 (2018).
 - [13] U. Percoco and V. M. Villalba, *Phys. Lett. A* **140**, 105 (1989).
 - [14] M. A. Hohensee, B. Estey, P. Hamilton, A. Zeilinger, and H. Müller, *Phys. Rev. Lett.* **108**, 230404 (2012).
 - [15] A. Zeilinger, R. Gähler, and M. A. Horne, *Phys. Lett. A* **154**, 93 (1991).
 - [16] Y. Aharonov, E. Cohen, and D. Rohrlich, *Phys. Rev. A* **93**, 042110 (2016).
 - [17] P. Pearle and A. Rizzi, *Phys. Rev. A* **95**, 052123 (2017).
 - [18] T. Maudlin, *Entropy* **20**, 465 (2018).
 - [19] B. Li, D. W. Hewak, and Q. J. Wang, *Found. Phys.* **48**, 837 (2018).
 - [20] Daniel F. Lima, Fabiano M. Andrade, Luis B. Castro, Cleverson Filgueiras, and Edilberto O. Silva, *The European Physical*

- Journal C **79**, 596 (2019).
- [21] A. N. Ikot, H. Hassanabadi, and T. M. Abbey, *Communications in Theoretical Physics* **64**, 637 (2015).
- [22] A. N. Ikot, S. Zarrinkamar, E. J. Ibanga, E. Maghsoodi, and H. Hassanabadi, *Chinese Physics C* **38**, 013101 (2014).
- [23] M. Hamzavi, A. Rajabi, and H. Hassanabadi, *Physics Letters A* **374**, 4303 (2010).
- [24] M. Hamzavi, A. A. Rajabi, and H. Hassanabadi, *Few-Body Systems* **48**, 171 (2010).
- [25] H. Hassanabadi, E. Maghsoodi, and S. Zarrinkamar, *Communications in Theoretical Physics* **58**, 807 (2012).
- [26] M. HAMZAVI, H. HASSANABADI, and A. A. RAJABI, *Modern Physics Letters A* **25**, 2447 (2010).
- [27] H. Hassanabadi, B. H. Yazarloo, and N. Salehi, *Indian Journal of Physics* **88**, 405 (2014).
- [28] Luis B. Castro and Edilberto O. Silva, *The European Physical Journal C* **75**, 321 (2015).
- [29] R. L. L. Vitória and K. Bakke, *International Journal of Modern Physics D* **27**, 1850005 (2018).
- [30] R. R. S. Oliveira, *General Relativity and Gravitation* **51**, 120 (2019).
- [31] K. Bakke and C. Furtado, *Ann. Phys. (Berlin)* **522**, 447 (2010).
- [32] M. M. Cunha, H. S. Dias, and E. O. Silva, *Phys. Rev. D* **102**, 105020 (2020).
- [33] E. O. Silva, S. C. Ulhoa, F. M. Andrade, C. Filgueiras, and R. G. G. Amarin, *Ann. Phys. (NY)* **362**, 739 (2015), 1502.07151.
- [34] F. M. Andrade, E. O. Silva, and M. Pereira, *Phys. Rev. D* **85**, 041701(R) (2012).
- [35] M. M. Cunha and E. O. Silva, *Advances in High Energy Physics* **2021**, 6709140 (2021).
- [36] R. R. S. Oliveira, A. A. Araújo Filho, F. C. E. Lima, R. V. Maluf, and C. A. S. Almeida, *The European Physical Journal Plus* **134**, 495 (2019).
- [37] H. Hassanabadi, S. Sargolzaeipor, and B. H. Yazarloo, *Few-Body Systems* **56**, 115 (2015).
- [38] B. C. Lütftüoğlu, J. Kříž, P. Sedaghatnia, and H. Hassanabadi, *The European Physical Journal Plus* **135**, 691 (2020).
- [39] A. N. Ikot, C. O. Edet, P. O. Amadi, U. S. Okorie, G. J. Rampho, and H. Y. Abdullah, *The European Physical Journal D* **74**, 159 (2020).
- [40] C. O. Edet, P. O. Amadi, M. C. Onyeaju, U. S. Okorie, R. Sever, G. J. Rampho, H. Y. Abdullah, I. H. Salih, and A. N. Ikot, *Journal of Low Temperature Physics* **202**, 83 (2021).
- [41] C. O. Edet, A. N. Ikot, M. C. Onyeaju, U. S. Okorie, G. J. Rampho, M. L. Lekala, and S. Kaya, *Physica E: Low-dimensional Systems and Nanostructures* **131**, 114710 (2021).
- [42] C. O. Edet and A. N. Ikot, *The European Physical Journal Plus* **136**, 432 (2021).
- [43] C. O. Edet, A. N. Ikot, U. S. Okorie, G. J. Rampho, M. Ramantswana, R. Horchani, H. Abdullah, J. A. Vinasco, C. A. Duque, and A.-H. Abdel-Aty, *International Journal of Thermophysics* **42**, 138 (2021).
- [44] F. M. Andrade and E. O. Silva, *Phys. Lett. B* **719**, 467 (2013).
- [45] P. Roy and R. Roychoudhury, *Phys. Lett. B* **359**, 339 (1995).
- [46] K. Bakke, E. O. Silva, and H. Belich, *J. Phys. G: Nucl. Part. Phys.* **39**, 055004 (2012).
- [47] K. Bakke and H. Belich, *The European Physical Journal Plus* **135**, 656 (2020).
- [48] H. Belich, E. O. Silva, J. Ferreira, M. M., and M. T. D. Orlando, *Phys. Rev. D* **83**, 125025 (2011).
- [49] A. G. de Lima, H. Belich, and K. Bakke, *Annalen der Physik* **526**, 514 (2014).
- [50] H. Aounallah and A. Boumali, *Physics of Particles and Nuclei Letters* **16**, 195 (2019).
- [51] A. Boumali and H. Aounallah, *Advances in High Energy Physics* **2018**, 1031763 (2018).
- [52] L. B. Castro and E. O. Silva, *Journal of Physics A: Mathematical and Theoretical* **51**, 035201 (2017).
- [53] Y. Yang, Z.-W. Long, H. Chen, Z.-L. Zhao, and C.-Y. Long, *Modern Physics Letters A* **36**, 2150059 (2021).
- [54] C. R. Hagen, *Phys. Rev. Lett.* **64**, 503 (1990).
- [55] V. Salem, R. F. Costa, E. O. Silva, and F. M. Andrade, *Front. Phys.* **7**, 175 (2019).
- [56] Armin Danner, Bülent Demirel, Wenzel Kersten, Hartmut Lemmel, Richard Wagner, Stephan Sponar, and Yuji Hasegawa, *npj Quantum Inf.* **6**, 1 (2020).
- [57] J. Ieda, M. Matsuo, and S. Maekawa, *Solid State Commun.* **198**, 52 (2014), sI: Spin Mechanics.
- [58] B. Mashhoon, *Entropy* **23**, 445 (2021).
- [59] J. Pétri, *Universe* **6**, 15 (2020).
- [60] Z. Stuchlík, M. Kološ, J. Kovář, P. Slaný, and A. Tursunov, *Universe* **6**, 26 (2020).
- [61] G. P. Zhang, Y. H. Bai, and T. F. George, *Phys. Rev. B* **104**, L100302 (2021).
- [62] A. M. Bubenchikov, M. A. Bubenchikov, A. V. Lun-Fu, and V. A. Ovchinnikov, *Eur. Phys. J. Plus* **136**, 1 (2021).
- [63] M. N. Chernodub, *Symmetry* **13**, 1569 (2021).
- [64] O. V. Kibis, H. Sigurdsson, and I. A. Shelykh, *Phys. Rev. B* **91**, 235308 (2015).
- [65] Mamoru Matsuo, Jun'ichi Ieda, Eiji Saitoh, and Sadamichi Maekawa, *Phys. Rev. B* **84**, 104410 (2011).
- [66] W. Bulla and F. Gesztesy, *J. Math. Phys.* **26**, 2520 (1985).
- [67] D. K. Park and J. G. Oh, *Phys. Rev. D* **50**, 7715 (1994).
- [68] Y. Aharonov and D. Bohm, *Phys. Rev.* **115**, 485 (1959).
- [69] C. R. Hagen, *Phys. Rev. A* **77**, 036101 (2008).
- [70] C. R. Hagen, *Phys. Rev. D* **48**, 5935 (1993).
- [71] F. M. Andrade, E. O. Silva, and M. Pereira, *Ann. Phys. (NY)* **339**, 510 (2013).
- [72] F. M. Andrade, E. O. Silva, T. Prudêncio, and C. Filgueiras, *J. Phys. G* **40**, 075007 (2013).
- [73] V. R. Khalilov, *Theor. Math. Phys.* **175**, 637 (2013).
- [74] V. Khalilov, *Eur. Phys. J. C* **73**, 2548 (2013).
- [75] V. Khalilov and C.-L. Ho, *Ann. Phys. (NY)* **323**, 1280 (2008).
- [76] V. Khalilov and I. Mamsurov, *Theor. Math. Phys.* **161**, 1503 (2009).
- [77] V. Khalilov, *The European Physical Journal C, Eur. Phys. J. C* **74**, 1 (2014).
- [78] C. Filgueiras, E. O. Silva, W. Oliveira, and F. Moraes, *Ann. Phys. (NY)* **325**, 2529 (2010).
- [79] Fabiano M. Andrade and Edilberto O. Silva, *Eur. Phys. J. C* **74**, 3187 (2014).
- [80] C. R. Hagen and D. K. Park, *Ann. Phys. (NY)* **251**, 45 (1996).
- [81] H. Nguyen, P. Meleshenko, A. Dolgikh, and A. Klinskikh, *The European Physical Journal D - Atomic, Molecular, Optical and Plasma Physics* **62**, 361 (2011).